Molecular Cell, Vol. 19, 405–419, August 5, 2005, Copyright ©2005 by Elsevier Inc. DOI 10.1016/j.molcel.2005.07.011

Crystal Structure of *A. aeolicus* Argonaute, a Site-Specific DNA-Guided Endoribonuclease, Provides Insights into RISC-Mediated mRNA Cleavage

Yu-Ren Yuan,[1] Yi Pei,[2] Jin-Biao Ma,[1] Vitaly Kuryavyi,[1] Maria Zhadina,[2] Gunter Meister,[2] Hong-Ying Chen,[1] Zbigniew Dauter,[3] Thomas Tuschl,[2,*] and Dinshaw J. Patel[1,*]
[1]Structural Biology Program
Memorial Sloan-Kettering Cancer Center
New York, New York 10021
[2]Laboratory of RNA Molecular Biology
The Rockefeller University
New York, New York 10021
[3]Synchrotron Radiation Research Section
National Cancer Institute
Argonne National Laboratory
Argonne, Illinois 60439

Summary

Argonaute (Ago) proteins constitute a key component of the RNA-induced silencing complex (RISC). We report the crystal structure of *Aquifex aeolicus* Ago (*Aa*-Ago) together with binding and cleavage studies, which establish this eubacterial Ago as a bona fide guide DNA strand-mediated site-specific RNA endonuclease. We have generated a stereochemically robust model of the complex, where the guide DNA-mRNA duplex is positioned within a basic channel spanning the bilobal interface, such that the 5′ phosphate of the guide strand can be anchored in a basic pocket, and the mRNA can be positioned for site-specific cleavage by RNase H-type divalent cation-coordinated catalytic Asp residues of the PIWI domain. Domain swap experiments involving chimeras of human Ago (hAgo1) and cleavage-competent hAgo2 reinforce the role of the PIWI domain in "slicer" activity. We propose a four-step Ago-mediated catalytic cleavage cycle model, which provides distinct perspectives into the mechanism of guide strand-mediated mRNA cleavage within the RISC.

Introduction

The RISC plays a key role in modulating eukaryotic gene expression through either chromatin remodeling, sequence-specific messenger RNA (mRNA) cleavage, or translational repression (Meister and Tuschl, 2004; Sontheimer, 2005; Tomari and Zamore, 2005). RISC-associated Ago proteins (Hammond et al., 2001; Cerutti et al., 2000; Carmell et al., 2002), with their PAZ domains and Piwi modules, contribute to the selection of the guide strand of small interfering RNAs (siRNAs) and subsequent targeting and cleavage of complementary mRNAs (Hutvagner and Zamore, 2002; Martinez et al., 2002).

Recent structures of the ~130 amino acid (aa) PAZ domain have been reported in the free form (Yan et al., 2003; Lingel et al., 2003; Song et al., 2003) as well as complexed with mononucleotide (Yan et al., 2003) and oligomeric RNA (Lingel et al., 2004; Ma et al., 2004). The PAZ domain adopts an Sm-like fold containing a basic binding cavity positioned between a central β barrel and an α helix/β hairpin segment. Structural studies at the protein-RNA complex level have identified the basis for ssRNA (Lingel et al., 2004) and siRNA-like (Ma et al., 2004) recognition by the PAZ domain.

The *piwi* gene encodes a highly basic ~300 aa segment, the Piwi module (Cerutti et al., 2000). In prokaryotes, proteins that contain Piwi modules also contain N-terminal extensions of unknown function. In eukaryotes, the Piwi module is found only in the Ago protein family associated with the RISC, which also contains an accompanying PAZ domain (Carmell et al., 2002). The recent crystal structures of *Archaeoglobus fulgidus* Piwi (*Af*-Piwi) protein (Parker et al., 2004) and *Pyrococcus furiosus* Ago (*Pf*-Ago) protein (Song et al., 2004) in the free state and *Af*-Piwi bound to siRNA (Parker et al., 2005; Ma et al., 2005) have advanced our understanding of the two-domain architecture of the Piwi module and its role in mediating functional events in the RNA silencing pathway (Liu et al., 2004; Rivas et al., 2005).

Song et al. (2004) have reported on the 2.25 Å crystal structure of *Pf*-Ago protein in the free state, thereby establishing that this archaeal Ago is composed of N, PAZ, Mid, and PIWI domains, with the PIWI domain shown to adopt a RNase H fold associated with a conserved DD-containing catalytic motif with potential for RNA cleavage activity. This group also proposed a model of siRNA-guided mRNA cleavage.

This paper reports on the 2.9 Å crystal structure of *Aa*-Ago protein, crystallized in the presence of single-stranded rU_8. This eubacterial Ago adopts a bilobal architecture composed of N and PAZ-containing and Mid and PIWI-containing lobes. Our binding and cleavage studies demonstrate that *Aa*-Ago is a site-specific DNA guide strand-mediated RNA endonuclease with highest affinity for DNA at the single-strand level and for DNA-RNA hybrid at the duplex level. We next generated a stereochemically robust model of a complex with a 21-mer DNA-RNA duplex anchored at the 5′ end of the DNA guide strand that, together with a four-step Ago-mediated catalytic cleavage cycle model, provides insights into the functional roles of the four domains for guide strand selection, mRNA alignment, and distance-dependent site-specific cleavage of mRNA target. These structural and modeling efforts on the *Aa*-Ago system, when combined with sequence alignments, have permitted identification of domain boundaries in hAgo proteins. The generation of chimeras through domain swapping between hAgo1 and cleavage-competent hAgo2 have independently confirmed that the PIWI domain is responsible for target mRNA cleavage activity (Liu et al., 2004; Rivas et al., 2005).

*Correspondence: ttuschl@mail.rockefeller.edu (T.T.); pateld@mskcc.org (D.J.P.)

Table 1. X-Ray Data, Phasing, and Refinement Statistics

Data Collection Statistics			
Space group $P2_12_12_1$			
Unit cell dimensions (Å): a = 63.92, b = 101.12, c = 115.07			
	SeMet		
	Peak	Inflection	Remote
Wavelength (Å)	0.9788	0.9790	0.95
Resolution (Å)	2.9	2.9	3.0
Redundancy	7.6	7.6	7.6
Unique Observations	31,931	32,001	29,069
Completeness (%) (last shell)	99.6 (98.6)	99.6 (99.3)	99.5 (99.2)
I/σ(I)	17.6 (2.6)	18.7 (2.7)	16.6 (2.2)
R_{sym} (%) (last shell)[a]	11.1 (47.2)	10.4 (47.1)	11.1 (56.0)
Phasing Statistics			
SeMet sites	6	6	6
Phasing power	1.324	1.342	1.136
Initial figure of merit	0.18 (40 Å ~ 2.9 Å)		
Refinement			
Resolution range (Å)	40 ~ 2.9		
R_{factor} (R_{free}) (%)[b,c]	21.2/30.0		
Rms bond length deviations (Å)	0.016		
Rms angles deviations (°)	1.836		
Percentage of core (allowed) in Ramachandran plot	87.5 (10.5)		

[a] R_{sym} is the unweighted R value on I between symmetry mates.
[b] $R_{factor} = \Sigma_{hkl}||F_{obs}(hkl)| - |F_{calc}(hkl)||\Sigma_{hkl}|F_{obs}(hkl)|$.
[c] R_{free} = the cross validation R factor for 5% of reflections against which the model was not refined.

Results

Crystallization and Structure Determination

The full-length *Aa*-Ago gene was amplified from *A. aeolicus* genomic DNA by PCR, with the protein next expressed in *E. coli* and subsequently purified to homogeneity. Crystals of *Aa*-Ago protein, successfully grown in the presence of rU_8, belong to the $P2_12_12_1$ space group, contain one molecule in the asymmetric unit, and diffract to 2.9 Å resolution. The structure was solved by multiple wavelength anomalous diffraction (MAD) on crystals of selenomethionine-labeled *Aa*-Ago protein, with crystallographic statistics summarized in Table 1.

Global Ago Architecture

The domain boundary and sequence alignment of *Aa*-Ago are summarized in Figures 1A and 1B, respectively. Two views of the *Aa*-Ago structure are shown in Figures 1C and 1D, with the overall bilobal architecture composed of 32 β strands (β1–β32) and 19 α helices (α1–α19) (Figure 1B). The N-terminal half (residues 4–305), designated the PAZ-containing lobe, is connected by a short linker segment to the C-terminal half (residues 318–706), designated the PIWI-containing lobe, The rU_8, required for successful crystallization, is disordered in the electron density map.

PAZ-Containing Lobe

The magenta-colored N domain (residues 1–108) is composed of an antiparallel four-stranded β sheet core with two α helices positioned along one face of the sheet and an extended β strand toward its N terminus (Figures 2A and 2B). The N domain core fold is most closely related to the catalytic domain of replication initiator (Rep) protein (Campos-Olivas et al., 2002) (Figure S1A available in the Supplemental Data with this article online). The green-colored linker L1 (108–166), which connects the N and PAZ domains, contains an α helix packed against a three-stranded antiparallel β sheet, with two long β stands (β8 and β9) of the sheet spanning one face of adjacent N and PAZ domains (Figures 2A and 2B). The cyan-colored PAZ domain (166–262) is composed of a mixed α/β scaffold containing a cleft bracketed by a pair of α helices on one side and a five-stranded β sheet and an α helix on the other (Figures 2A and 2B). The PAZ core fold is closely related to the human hAgo1 PAZ domain, except that a pair of α helices (α5 and α6) replace an α helix/β hairpin scaffold (Ma et al., 2004) (Figure S1B). The N, L1, and PAZ domains are arranged in a triangular arrangement (Figure 2B), with each domain interacting with the other two domains. The yellow-colored linker L2 (262–312) starts with two α helices aligned orthogonal to each other (Figures 2A and 2B) followed by a β strand involved in connecting the two lobes of the bilobal *Aa*-Ago architecture (Figures 1C and 1D). Linker L2 together with N, L1, and PAZ form a compact global fold (Figure 2B). One surface of the PAZ-containing lobe, that directed toward the PIWI-containing lobe and corresponding to the view in Figure 2B, exhibits a pronounced basic electrostatic surface (Figure 2C).

PIWI-Containing Lobe

The yellow-colored linker L2 (residues 312–335) at the start of the C-terminal PIWI-containing lobe consists of extended segments on either side of a short β sheet (Figures 2D and 2E). The magenta-colored Mid domain (335–488) is composed of a parallel four-stranded β sheet core, surrounded by four α helices and two addi-

tional short α helices (Figures 2D and 2E). The Mid core fold is closely related to the amino terminal tryptic core fragment of the *E. coli* lactose repressor (Friedman et al., 1995) (Figure S2A). The cyan-colored PIWI domain (488–706) contains a central six-stranded mixed β sheet surrounded by four α helices (Figures 2D and 2E). The PIWI core fold of *Aa*-Ago is closely related to the RNase HII domain (Lai et al., 2000) (Figure S2B). There exists an extensive interface between the Mid and PIWI domains (Figure 2E). One surface of the PIWI-containing lobe, that directed toward the PAZ-containing lobe and corresponding to the view in Figure 2E, exhibits a pronounced basic electrostatic surface (Figure 2F), with its most basic segment lining the periphery of a potential binding pocket (red arrow in Figure 2F).

The N Domain Projects a Basic Surface Patch for Putative RNA Recognition

One surface of the N domain, which is directed across a narrow groove toward the adjacent PAZ domain, presents a patch of basic residues (K34, K37, and R41) projecting off one face of an α helix (α1) (Figure 3A), with the potential for participating in RNA-mediated interactions.

The PAZ Domain Contains a 3′ Overhang Binding Pocket

Previous structural studies of PAZ-RNA recognition have established that RNA 3′ overhang (OH) ends can be positioned within a hydrophobic and aromatic residue-lined cleft of the PAZ domain (Yan et al., 2003; Lingel et al., 2004; Ma et al., 2004). *Aa*-Ago PAZ residues F209, W226, and R195 are conserved amongst Ago sequences (Figure 1B) and occupy similar spatial positions with their counterparts in other PAZ domains (Figure S3), implying similar functional roles in potentially binding the 3′ end (F209 and W226) and in orienting the backbone (R195) of the guide RNA.

The Mid Domain Contains a Binding Pocket for 5′ Phosphate of the Guide Strand

The C-terminal half of the Mid domain and the entire PIWI domain of *Aa*-Ago span the ~300 aa region previously assigned as the boundaries of the Piwi module (Cerutti et al., 2000). The conserved C-terminal half of the Mid domain has extensive interactions with the PIWI domain, with a deep basic pocket positioned on the surface of the Mid domain adjacent to the interface with the PIWI domain (Figure 3C), as first reported by Parker et al. (2004) for the *Af*-Piwi protein in the free state. This deep basic surface pocket (shown by the red arrow in Figure 2F) is lined by highly conserved residues, including an aromatic residue (Y439), a patch of basic residues (K443, R444, and K480, represented by blue side chains in Figures 2D and 2E), and polar residues (Q454 and Q476) from the Mid domain, supplemented by the C-terminal carboxylate and conserved aromatic residue (Y681), contributed to the Mid-PIWI interface by the PIWI domain (Figure 3C).

More recently, the crystal structures of *Af*-Piwi-RNA complexes (Parker et al., 2005; Ma et al., 2005) have definitively established that the phosphorylated 5′ end of the guide RNA is anchored within this highly conserved basic pocket, implying that this pocket is also likely to be the site for 5′ end recognition of the guide strand in Ago proteins.

The PIWI Domain Contains an mRNA Cleavage Site

The first indications that the PIWI domain adopts an RNase H fold containing a catalytic DD-containing motif emerged from the crystal structures of *Pf*-Ago (Song et al., 2004) and *Af*-Piwi (Parker et al., 2004) proteins. The RNase H-like scaffold of the PIWI domain of *Aa*-Ago projects three highly conserved acidic amino acids (D502, D571, and E578), with the Asp residues directed toward a divalent Ca^{2+} cation (red side chains and orange ball in Figures 2D, 2E, and 3D). D502 is coordinated to the divalent cation, whereas E578 is furthest from the divalent cation, from which it is separated by the conserved basic residue R570. The spatial organization of the DD-containing motif projecting from the RNase H scaffold of the PIWI domain of *Aa*-Ago matches the corresponding DDE motif projecting from RNase HII (Lai et al., 2000) (Figure S2B) as well as related motifs in integrases, reverse transcriptases, and transposases (Yang and Steitz, 1995). Furthermore, nonconserved D683 is positioned near conserved D502 and participates in coordinating the bound Ca^{2+} cation.

Because RNase H is a divalent cation-dependent enzyme that specifically cleaves DNA-RNA hybrid duplexes, the observation of a bound Ca^{2+} coordinated by D502 of the conserved DD-containing motif and D683 of *Aa*-Ago immediately points toward involvement of elements of the DD-containing motif in mRNA cleavage activity, as first proposed from the structure of *Pf*-Ago (Song et al., 2004) and verified from mutation studies of hAgo2 (Liu et al., 2004).

"PIWI Box" Pairs with Linker Connecting Two Lobes of the Ago Scaffold

The "PIWI box" corresponds to a conserved ~40 aa segment nestled within the highly basic ~300 aa Piwi module (Cerutti et al., 2000). The *Aa*-Ago PIWI box (Figures 2D and 2E), composed of three β strands (β29, β30, and β31), occupies a position close to the pivot point linking the two hemispheric lobes of the *Aa*-Ago scaffold (Figures 1C and 1D) and, given its surface positioning, is available for recognition (Tahbaz et al., 2004).

Filter Binding Assays of *Aa*-Ago-Nucleic Acid Complex Formation

The double filter binding assay (Wong and Lohman, 1993) was used to test the binding affinity and specificity of *Aa*-Ago for DNA and RNA oligonucleotides. Unexpectedly, *Aa*-Ago bound more tightly to 21-mer ssDNA (0.01 μM) compared to 21-mer ssRNA (0.97 μM) (Figures 4A and 4B). A similar trend was observed at the 21-mer duplex level, where binding affinity was stronger for complexes with DNA-RNA (0.64 μM) and DNA-DNA (1.01 μM) duplexes compared to RNA-RNA duplexes (>10 μM) (Figures 4A and 4B).

We observed similar activities in competition assays for single-stranded 21-mer RNAs with and without a 5′ phosphate (Figure 4C). Similarly, introduction of the bulky fluorescein group at the 5′ end and the bulky bio-

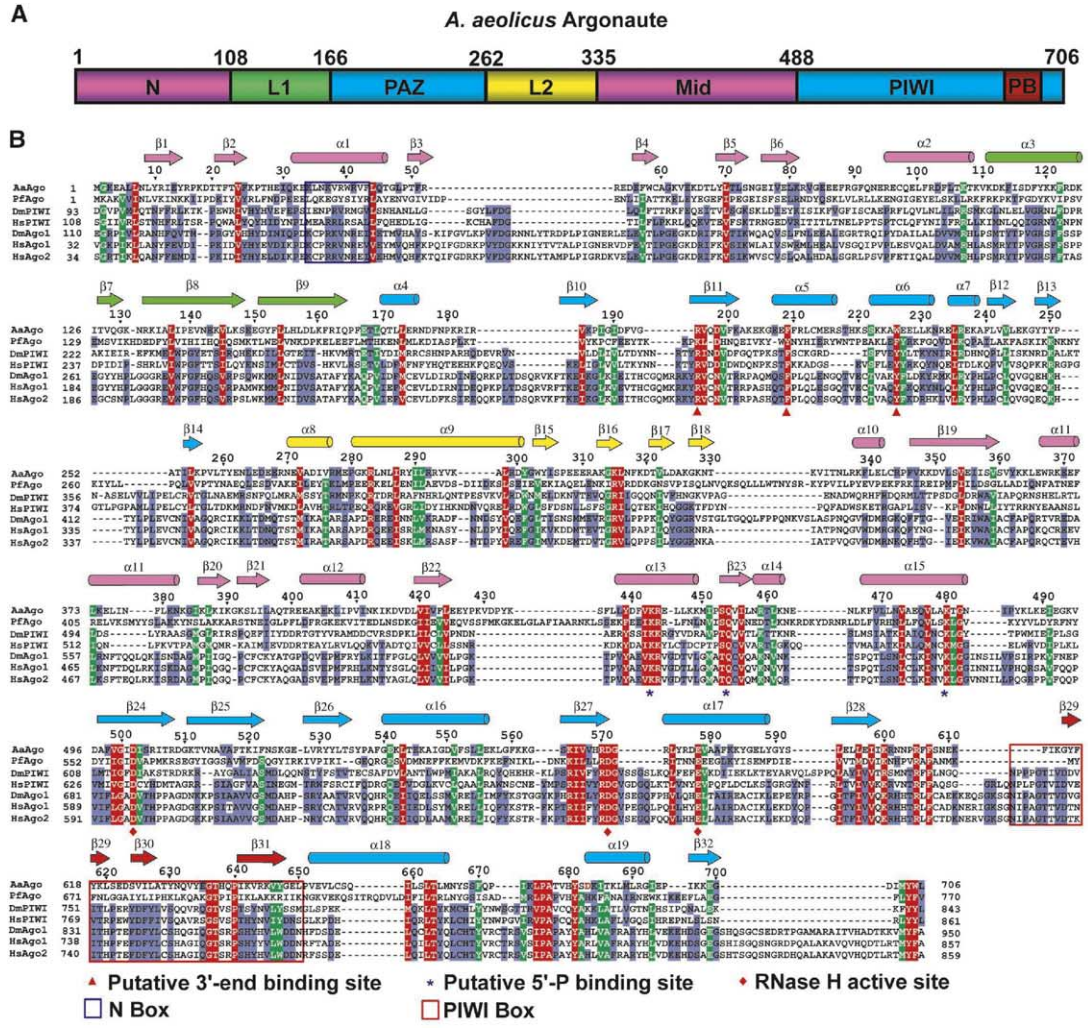
A
A. aeolicus Argonaute
1
108
166
262
335
488
706
N
L1
PAZ
L2
Mid
PIWI
PB
B
AaAgo
PfAgo
DmPIWI
HsPIWI
DmAgo1
HsAgo1
HsAgo2
Putative 3'-end binding site
Putative 5'-P binding site
RNase H active site
N Box
PIWI Box

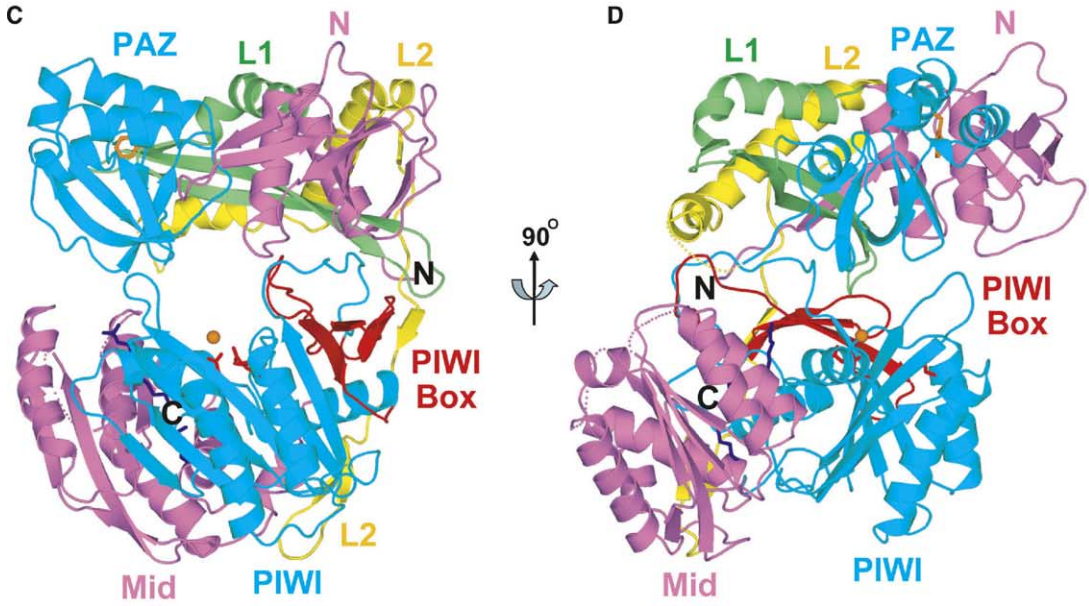
C
PAZ
L1
N
L2
N
PIWI
Box
C
L2
Mid
PIWI
90°
D
L1
L2
PAZ
N
N
PIWI
Box
C
Mid
PIWI

tin group at the 3′ end had no effect on the binding activity in the competition assay (Figure 4C).

The PIWI Domain of hAgo2 Is Required for mRNA Cleavage

Earlier findings have demonstrated that only hAgo2, but not hAgo1, hAgo3, and hAgo4, is able to guide cleavage of a complementary target RNA (Meister et al., 2004; Liu et al., 2004). An intact hAgo2 was required for its cleavage activity, and the active site of hAgo2 is located in its PIWI domain. As an initial attempt to reveal the unique structural features of hAgo2, we performed domain-swapping experiments between hAgo2 and hAgo1 (Figures 4D and 4E). The FLAG/HA-tagged swapped mutants were transiently expressed in 293 HEK cells, immunoprecipitated, and assayed for their cleavage activity. The chimerical Ago proteins containing the PIWI domain of hAgo2, either alone or paired with the hAgo2 Mid domain, were capable of small RNA-guided cleavage of target RNA (Figure 4E, lanes 6 and 4). On the other hand, the chimerical Ago proteins containing the PIWI domain of hAgo1 showed no cleavage activity (Figure 4E, lanes 5 and 7). Our results not only reinforce earlier observations that the DD-containing motif within the PIWI domain of hAgo2 is the prominent determinant for its unique cleavage activity (Song et al., 2004; Liu et al., 2004; Rivas et al., 2005) but also highlight the unique microenvironment restricted to this domain in hAgo2.

Aa-Ago Is a Bona Fide Site-Specific RNA Endonuclease

To test for cleavage activity of the *Aa*-Ago protein, we preincubated recombinantly expressed *Aa*-Ago protein with single-stranded 5′ phosphorylated 18, 21, or 24 nt DNA or RNA oligonucleotides and then added 5′-^{32}P cap-labeled RNA substrate. We examined different divalent metal ions and different temperatures. Cleavage of the target RNA was not detectable in the presence of Ca^{2+}, but cleavage was detectable in the presence of Mg^{2+} for DNA and Mn^{2+} for both DNA and RNA (Figure 5). DNA as the guide strand was much more active than RNA, and the variation of the length of the guide strand from 18- to 24-mer had little effect on the position or efficiency of target RNA cleavage. Cleavage activity was most pronounced at 55°C, which may not be surprising given that *Aquifex aeolicus* is a thermophilic bacterium. At 75°C, the cleavage activity of *Aa*-Ago still persists, albeit nonspecific hydrolysis of the substrates was prominent (data not shown).

Stereochemically Robust Model of *Aa*-Ago Bound to a Guide DNA-mRNA Duplex

Our modeling efforts have focused on *Aa*-Ago complexes with duplexes formed by pairing of a guide DNA strand with an mRNA strand, given the findings of the double filter binding (Figure 4B) and cleavage (Figure 5) assays. We have successfully docked the guide DNA-mRNA duplex into a stereochemically compatible basic channel within the *Aa*-Ago scaffold by positioning the 5′ phosphate of the guide DNA strand within the 5′ end recognition pocket of the Mid domain, as well as locating the scissile mRNA phosphate near the Ca^{2+}-coordinated DD-containing motif of the RNase H scaffold of the PIWI domain, while keeping DNA-RNA duplex in a standard helical form. Steric clashes were relieved by interactive modeling, which primarily required repositioning of linker L1 and reorientation of the PAZ domain. The resulting docking model was next refined by using molecular dynamics calculations to yield a stereochemically robust model of the complex. The details of the modeling protocols are outlined in the Experimental Procedures.

Two views of this model of the complex are shown in Figures 6A and 6B, with the guide DNA strand in red and the mRNA strand in blue, positioned between the basic electrostatic surfaces of the two mutually facing N-terminal (Figure 2C) and C-terminal (Figure 2F) lobes. A comparison of the modeled *Aa*-Ago complex (Figures 6A and 6B) with the structure of the free *Aa*-Ago protein (Figures 1C and 1D) establishes a somewhat increased separation of the N- and C-terminal lobes of the bilobal Ago architecture and a pronounced rotational/translational movement of the PAZ domain away from the N domain on complex formation.

The positioning of the 5′ end of the DNA guide strand in the basic Mid binding pocket is shown in Figure S4A, whereas positioning of the scissible phosphate on the mRNA strand proximal to the catalytic Ca^{2+}-coordinated DD-containing motif of the RNase fold of the PIWI domain is shown in Figure S4B. The accessibility of the 5′ end of the DNA guide strand for pairing with the mRNA strand can be assessed from viewing the top half of the duplex in Figure S4C, whereas the positioning of the bottom half of the duplex between the spaced-apart N and PAZ domains is shown in Figure S4D.

There are extensive contacts between the protein and both the major (Figure S5A) and minor (Figure S5B) grooves of the guide DNA-mRNA duplex in the energy-minimized model of the *Aa*-Ago complex, and these in-

Figure 1. Sequence Alignment and Crystal Structure of *Aa*-Ago

(A) Domain and linker topology of the *Aa*-Ago.

(B) Sequence alignment of Ago domains. The aligned sequences (Genebank ID, designated gi) are in the order of *Aquifex aeolicus*-1147 (AaAgo, gi:5606619), *Pyrococcus furiosus*-0537 (PfAgo, gi:18976909), *Drosophila* PIWI (DmPIWI, gi:17136736), human PIWI (HsPIWI, gi:18098558), *Drosophila* Argonaute1 (DmAgo1, gi:17647145), human Argonaute1 (HsAgo1, gi:6912352), and human Argonaute2 (HsAgo2, gi:29171734). The secondary structure diagram for *Aa*-Ago is shown on the top, color coded by domains and linkers. Conserved residues are shaded in blue (60% conservation) and green (80% conservation), whereas essentially invariant residues are shaded in red.

(C) A view of the overall bilobal architecture of *Aa*-Ago. The domains and linkers are color coded as in (A).

(D) An alternate view of *Aa*-Ago rotated counter-clockwise by 90° along the z axis.

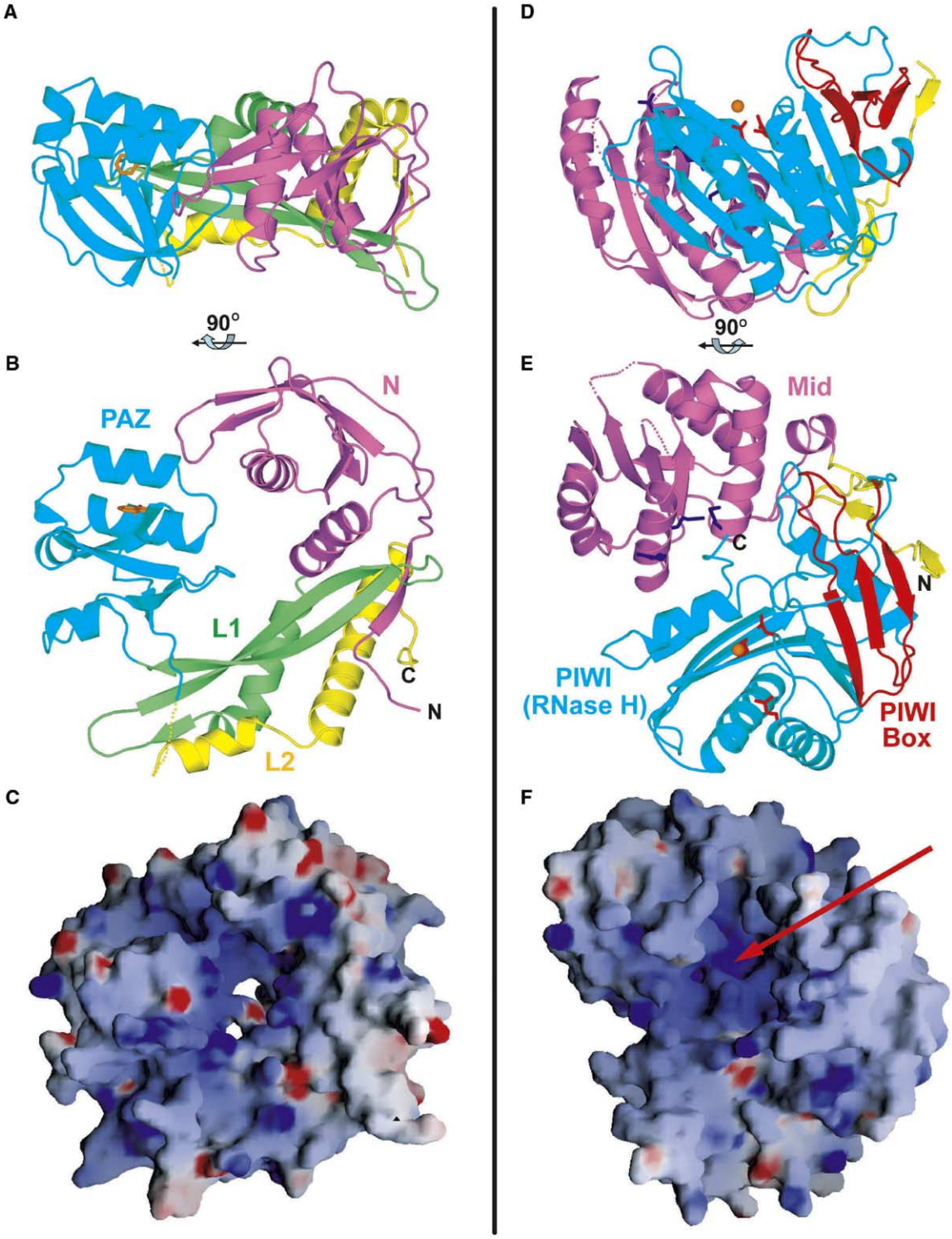

Figure 2. Domain Alignments within the PAZ-Containing (1–311) and PIWI-Containing (312–706) Lobes of *Aa*-Ago

(A) The PAZ-containing lobe is oriented as in Figure 1C with the N (1–108) and PAZ (166–262) domains in magenta and cyan, respectively, whereas the linkers L1 (residues 108–166) and L2 (262–311) are in green and yellow, respectively. A conserved tryptophan (W226) within the PAZ pocket is shown in orange.

(B) Clockwise rotation of (A) along the y axis showing the face of the PAZ-containing lobe positioned to interact with its counterpart on the face of the PIWI-containing module lobe.

(C) GRASP-based electrostatics view of (B) highlighting surface basic patches (colored blue).

(D) The PIWI-containing module is oriented as it is in Figure 1C with the linker L2 (312–334) in yellow and the Mid (335–488) and PIWI (488–706) domains in magenta and cyan, respectively, whereas the PIWI box (622–650) is colored red. Conserved acidic amino acids (D502, D571,

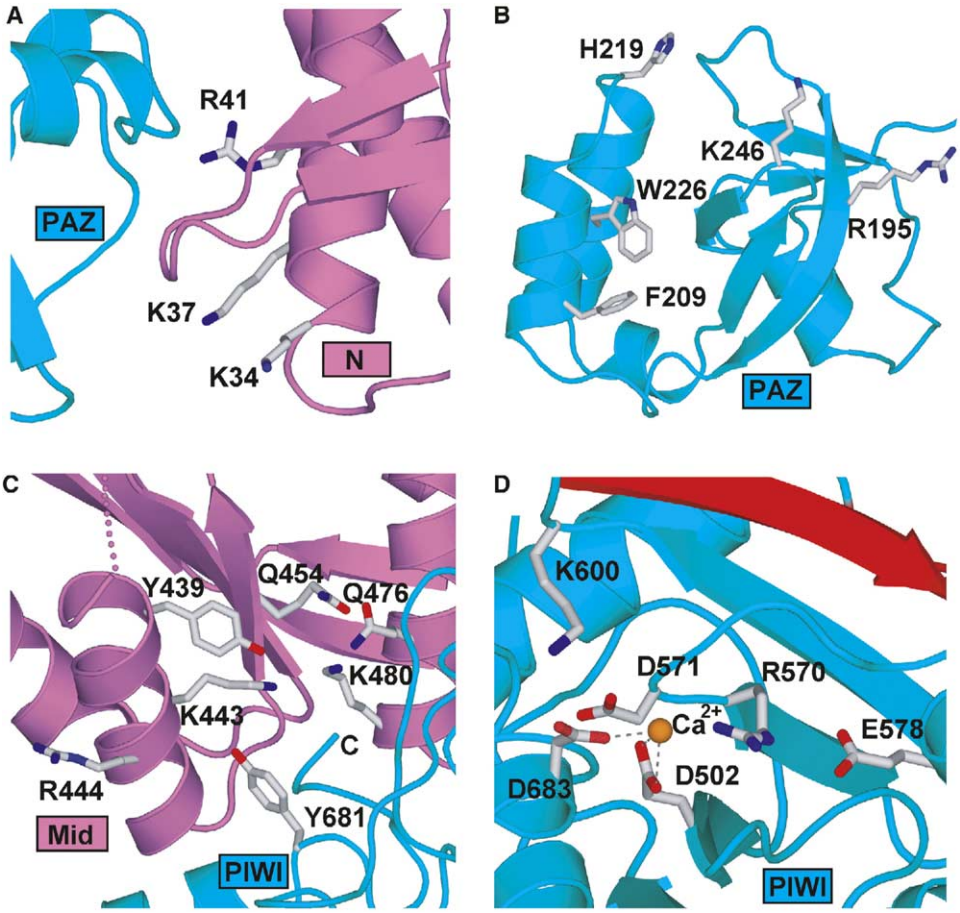

Figure 3. Positioning of Key Residues in the N, PAZ, Mid, and PIWI Domains of *Aa*-Ago

(A) Relative positions of basic K34, K37, and R41 residues on the surface of the N domain across from the PAZ domain.

(B) Conserved aromatic residues F209, H219, and W226 lining the 2 nt 3′ OH binding pocket and conserved basic residues R195 and K246 on the RNA binding surface of the PAZ domain.

(C) Relative positioning of conserved basic K443, R444, and K480 and polar Q454 and Q476 residues, candidates for anchoring the 5′ phosphate of the guide strand, within a pocket on the Mid domain. Also shown are aromatic residues Y439 and Y681 that line this potential recognition pocket.

(D) Relative positioning of invariant catalytic acidic D502, D571, and E578 residues and bound Ca^{2+} cation on the surface of the RNase H fold of the PIWI domain. Invariant basic R570 is also positioned in the catalytic pocket, whereas conserved basic K600 is directed toward the catalytic pocket. The Ca cation is also coordinated by D683, which is an Arg residue in hAgo1 and a His residue in hAgo2.

termolecular contacts are discussed in the Supplemental Data.

Discussion

Comparison of *Aa*-Ago and *Pf*-Ago Scaffolds

The same domains and linkers are observed in sequential order and relative orientation in the global architectures of both *Aa*-Ago (Figures 1C, 1D, and 2 and Figure S6A) and *Pf*-Ago (Figure S6B) (Song et al., 2004). Nevertheless, there are substantial local differences between structures and also different perspectives related to relative alignments of the individual domains. First, we visualize the *Aa*-Ago structure (Figures 1C and 1D and Figure S6A) as a [2 + 2] bilobal architecture defined by PAZ-containing (N and PAZ domains) and PIWI-containing (Mid and PIWI domains) lobes connected by a short hinge element. By contrast, the *Pf*-Ago structure (Figure S6B) has been visualized as an [1 + 3] architecture, where the PAZ domain is positioned over a cres-

and E578) within the RNase H fold of the PIWI domain are shown in red with a coordinated divalent Ca^{2+} cation in orange. Conserved basic amino acids (K443, R444, and K480) within the Mid domain, which are candidates for anchoring the 5′-phosphate of the guide strand, are shown in blue.

(E) Counter-clockwise rotation of (D) along the y axis showing the face of the PIWI-containing lobe positioned to interact with its counterpart on the face of the PAZ-containing lobe.

(F) GRASP-based electrostatics view of (E) highlighting basic patches (colored blue), with the most basic segment highlighted by a red arrow.

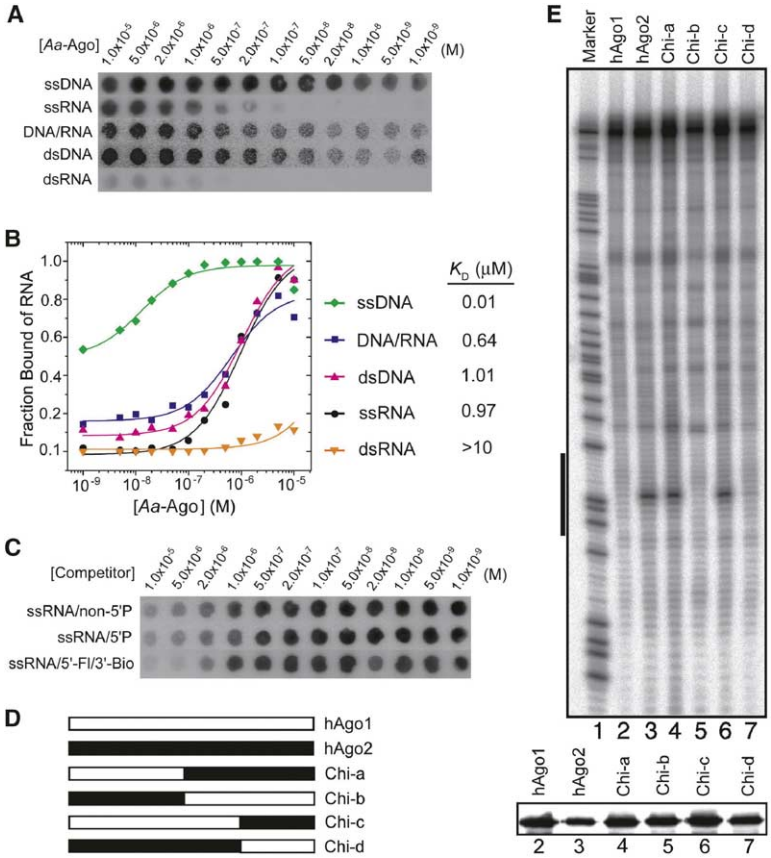

Figure 4. Nucleic Acid Double Filter Assays of *Aa*-Ago and Cleavage Assays of Chimeric hAgo1 and hAgo2 Constructs

(A) X-ray images of the nitrocellulose Protran BA-85 membrane (binds protein) and Nylon HyBond-N+ membrane (binds nucleic acids) in the double filter binding assay where various ^{32}P-labeled nucleic acids bound *Aa*-Ago with concentrations increasing from left (1×10^{-9} M) to right (1×10^{-5} M).

(B) The binding curves for *Aa*-Ago with various nonself-complementary nucleic acid ligands (Table S1), which are ^{32}P-labeled at their 5′ ends. The deduced apparent K_D values are listed on the right.

(C) X-ray images of the nitrocellulose Protran BA-85 membrane and Nylon HyBond-N$^+$ membrane in the competitive binding assay starting from *Aa*-Ago bound to a 5′-phosphorylated 21-mer RNA. The concentration of competitor decreased from left (1×10^{-5} M) to right (1×10^{-9} M).

(D) Schematic showing design of chimerical constructs associated with domain swapping experiments between hAgo1 and hAgo2. Chi-a and Chi-b are the chimerical proteins resulting from swapping both Mid and PIWI domains of hAgo1 and hAgo2; Chi-c and Chi-d are the chimerical proteins resulting from swapping of only the PIWI domain of the hAgo1 and hAgo2.

(E) FLAG/HA-tagged hAgo1, hAgo2, and chimerical proteins purified from HEK 293 cells were reconstituted by using single-stranded siRNA and subsequently incubated with ^{32}P cap-labeled target RNA. The cleavage products were resolved by 8% denaturing RNA-PAGE, and radioactivity was detected by phosphorimaging. The black bar to the left side of the image represents the region of the target RNA complementary to utilized guide RNA. The expression levels of the proteins used in the assays were assessed by Western blotting using anti-HA antibody and are shown in the lower panel.

cent-shaped scaffold composed of the remaining three domains (Song et al., 2004). These contrasting architectures identify different linkers as hinge regions contributing to interdomain flexibility. Second, the *Aa*-Ago PAZ domain adopts a "closed" architecture with an α-helical pair (α5, α6) subdomain positioned over the central β barrel (Figure S6A), whereas the *Pf*-Ago PAZ structure adopts an "open" architecture, resulting in a ~60° rotation, with the α-helical pair subdomain flipped out from the central β barrel (Figure S6B). Third, our *Aa*-Ago structure has a narrow channel between the N and PAZ domains and a wide channel between the PAZ and PIWI domains, with the opposite trend observed in the *Pf*-Ago structure. Fourth, a Ca^{2+} cation is observed proximal to the Asp residues of the DD-containing catalytic cleavage motif of the RNase H fold in *Aa*-Ago, but only a bound water molecule was initially observed in *Pf*-Ago. More recently, an Mn^{2+} cation has been soaked into the crystal of *Pf*-Ago and coordinates with the two catalytic Asp residues (Rivas et al., 2005).

DNA Guide Strand Binding and mRNA Cleavage Activities of Bacterial Ago Proteins

An important feature of *Aa*-Ago is its preference for binding to ssDNA over ssRNA and for DNA-containing duplexes over RNA-RNA duplexes (Figures 4A and 4B). A similar preference for DNA over RNA was also observed for binding by nucleic acids of the archaeal *Af*-Piwi protein (Ma et al., 2005). These unanticipated findings open new avenues for future investigation of the role of guide DNA in mediating the functional activities of eubacterial and archaeal Ago proteins, perhaps in Ago-mediated chromatin remodeling events.

The observation that a bacterial Ago protein is able to function as an RNA endonuclease by using a DNA guide strand might suggest that other Piwi family Ago proteins, including the human Piwi subfamily, may also possibly use DNA rather than RNA as guide strands. It will be important in the future to determine associated small DNA or RNA molecules and determine their function and the biological processes in which they are involved.

Guide Strand 5′ End Recognition by the Mid Domain

A key feature of our model of guide DNA-mRNA bound *Aa*-Ago complex involves anchoring of the 5′ end (Parker et al., 2005; Ma et al., 2005), especially the 5′ phosphate of the guide strand within a basic pocket involving highly conserved Lys and Gln residues of the Mid domain, as well as the divalent cation-coordinated C-terminal carboxylate of the PIWI domain (Figure S4A). The base at position 1 of the guide strand is not paired with its complementary partner on mRNA but rather stacks on Y439, with the backbone making a U turn such that the nonbridging oxygens of the 5′ phos-

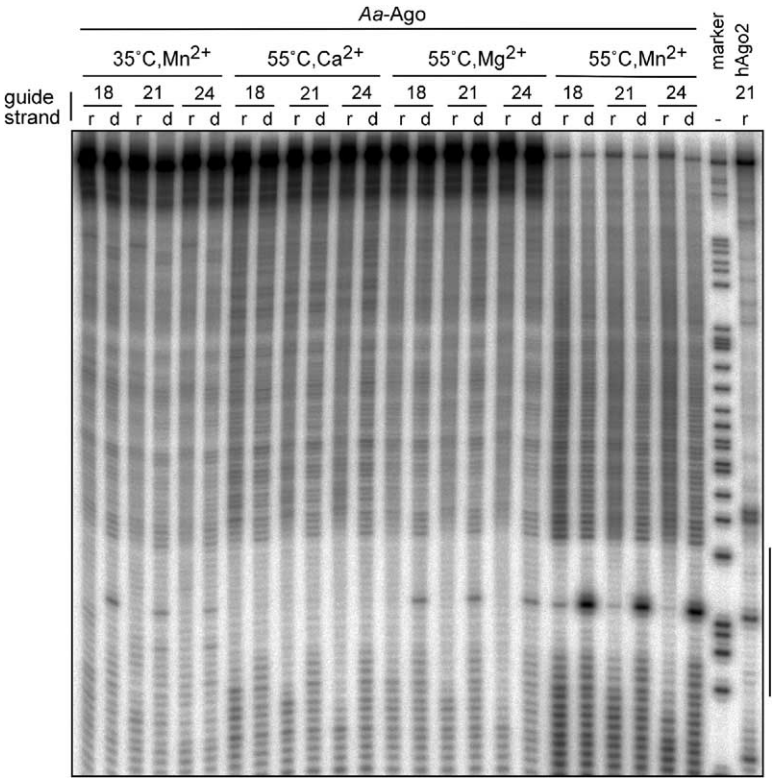

Figure 5. Target RNA Cleavage Activity of *Aa*-Ago

Recombinant *Aa*-Ago was assayed for cleavage of ^{32}P cap-labeled target RNA after reconstituted with ssRNA (r) or ssDNA (d) of variant length (18-, 21- and 24-mer) in the presence of indicated divalent cation cofactor at either 35°C or 55°C. As a control, human recombinant Ago2 was also assayed for cleavage activity at 35°C in the presence of magnesium after reconstituted with 21-mer ssRNA. After treatment with proteinase K, the cleavage products were resolved on an 8% denaturing PAGE gel and radioactivity was detected by phosphorimaging. The black bar to the right side of the image represents the region of the target RNA complementary to the 21 nt guide strand.

phate and the next-nearest-neighbor phosphate are brought in close proximity to coordinate the divalent cation (Figure S4A). This result is consistent with biochemical and kinetic measurements that established that the first base pair is often predicted to be unpaired within miRNA-mRNA duplexes in RISC (Lewis et al., 2003), that cleavage activity was independent of base pair disruption at this site, and that indeed such site-specific base pair disruption could even favor target cleavage under certain conditions (Haley and Zamore, 2004).

In our model of the complex, the phosphates of five consecutive residues (positions 2–6) toward the 5′ end of the guide strand, which adopt a helical pitch, have extensive surface and charge complementarity with side chains projecting from the PIWI and a portion of the Mid domains (Figure 6C). This suggests that the 5′ end of the guide strand could bind *Aa*-Ago in a stacked helical conformation both in the absence and presence of the partner mRNA strand. There is considerable biochemical evidence in the literature supporting the concept of a preorganized helical conformation at the 5′ end of the guide strand (Lewis et al., 2003, 2005; Doench et al., 2003; Doench and Sharp, 2004; Haley and Zamore, 2004).

Accessibility of 5′ End of Guide Strand for mRNA Alignment

The 5′ end of the guide strand is accessible for pairing with the mRNA in our model of the *Aa*-Ago complex (Figure S4C), consistent with similar observations in the crystal structures of the *Af*-Piwi-siRNA complex (Parker et al., 2005; Ma et al., 2005). Thus, the Watson-Crick edges of nucleotides 2–8 of the guide strand are directed outward into solvent, thereby providing easy access for recognition by mRNA targets. These conclusions provide support for the concept that mRNA initially nucleates with the 5′ end of the protein bound guide strand (Stark et al., 2003; Mallory et al., 2004; Doench and Sharp, 2004). Indeed, previous studies have shown that bases near the guide strand 5′ end contribute disproportionately to target RNA binding energy (Haley and Zamore, 2004) and that complementarity of the mRNA with the 5′ end of the guide RNA is more critical than complementarity with the 3′ end in translational repression (Doench and Sharp, 2004).

Our filter binding competition assays demonstrate that the binding affinities of single-stranded 21-mer RNAs for *Aa*-Ago are independent of the 5′ end being OH, or phosphate, or bulky fluorescein modification (Figure 4C), suggesting that there may be more than one conformation accessible to the 5′ end on complex formation. These results suggest that 5′ phosphate recognition may be important as a proof-reading step for recognition of the duplex siRNA before unwinding and loading of the single-stranded guide siRNA into the RISC. Recent results with hAgo2 have demonstrated that the 5′ phosphate is important for fidelity, but not critical for creation of an active enzyme (Rivas et al., 2005).

mRNA Cleavage Site within *Aa*-Ago PIWI Domain

The RNase H-like scaffolds of the PIWI domain of *Pf*-Ago (Song et al., 2004), *Af*-Piwi (Parker et al., 2004), and *Aa*-Ago proteins, and their divalent cation-coordinated DD-containing motifs, have striking similarities in the

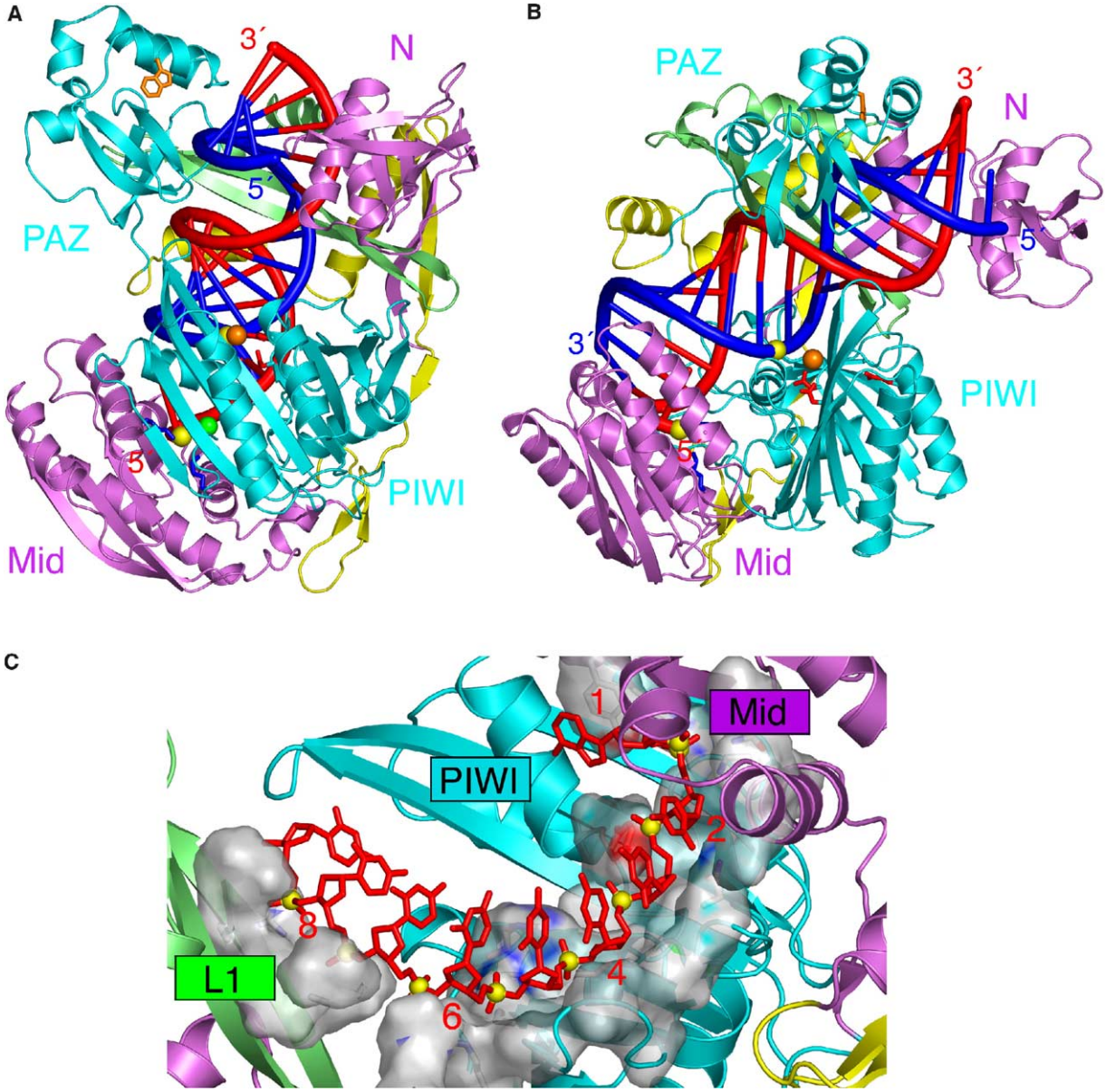

Figure 6. Stereochemically Robust Model of *Aa*-Ago Bound to Guide DNA-mRNA

(A) A view of the model of the complex with the same perspective as the free *Aa*-Ago shown in Figure 1C. The hybrid duplex between the guide DNA strand (colored red) and the mRNA strand (colored blue) is shown in a tubular representation, with a thicker diameter for the sugar-phosphate backbone and thinner diameter for the bases.

(B) A view of the model of the complex with the same perspective as the free *Aa*-Ago shown in Figure 1D.

(C) The phosphodiester backbone corresponding to positions 2–8 from the 5′ end of the guide strand are positioned within a trough-like segment of the Mid and PIWI domains in the model of the complex. The guide strand is shown in red, with phosphorus atoms as yellow balls. The trough is shown in a surface representation and exhibits surface complementarity with the sugar-phosphate backbone of the 5′ end region of the guide strand.

positioning of acidic and aromatic residues with human (Lima et al., 2003) and *Saccharomyces cerevisiae* (Evans and Bycroft, 1999) RNase HI. Further, the products of RISC-mediated mRNA cleavage, namely a 3′ hydroxyl and a 5′ phosphate (Martinez and Tuschl, 2004, Schwarz et al., 2004), are also the products after RNase H cleavage of the RNA strand of a DNA-RNA hybrid duplex.

Unlike Tn5 transposase (Davies et al., 2000), where all three residues in the DDE catalytic triad are critical for cleavage activity, only D502 and D571 in *Aa*-Ago are close to the Ca^{2+} ion, whereas E578 is separated from the divalent cation. This implies that only the DD component is likely to be important for catalytic cleavage in *Aa*-Ago, as recently demonstrated experimentally for hAgo2, where substitution of Ala for the conserved ca-

talytic Asp residues resulted in retention of binding but loss of cleavage activity in both in vitro and in vivo experiments (Liu et al., 2004). In addition, D683 is also coordinated to the Ca^{2+} ion in *Aa*-Ago, with the equivalent position occupied by H807 in hAgo2. Recent point mutation studies have shown that H807, as part of a DDH motif, contributes to hAgo2 phosphodiester cleavage chemistry (Rivas et al., 2005).

The Piwi-containing module (PIWI and Mid domains) exhibits substantial surface and charge complementarity with the guide DNA-mRNA duplex in our model of the complex. This complementarity most likely contributes to the proper alignment of the duplex with respect to the catalytic cleavage residues positioned within the PIWI domain. Simultaneous recognition of both the minor and major groove in the vicinity of the cleavage site (Figure S5) could restrict binding within this region to regular helical duplexes in the *Aa*-Ago complex, consistent with previous results stressing the importance of an A-form conformation within the RISC active site for cleavage activity (Chiu and Rana, 2003).

The PIWI Domain Is Responsible for Cleavage Competence of hAgo2

Of the four characterized hAgo proteins, only hAgo2 is competent for catalytic cleavage of the mRNA in the RISC (Meister et al., 2004; Liu et al., 2004). This provided an opportunity to undertake domain swap experiments involving hAgo1 and hAgo2 to identify the domain responsible for cleavage activity. The results outlined in Figure 4E unambiguously establish and reinforce earlier conclusions (Liu et al., 2004) that the PIWI domain is the cleavage-competent module within hAgo2. Because both catalytically competent (hAgo2) and incompetent (hAgo1, hAgo3, and hAgo4) proteins contain common DD residues of the catalytic motif within the RNase H fold, additional amino acids lining the catalytic pocket may contribute to cleavage activity. In this regard, H807 of Ago2 has been recently shown to influence catalytic cleavage (Rivas et al., 2005).

The Helical Distance Ruler Defines the mRNA Cleavage Site

Previous biochemical studies have established site-specific cleavage of the mRNA strand between positions 10 and 11, as defined from the 5′ end of the guide strand, within the RISC (Elbashir et al., 2001a, 2001b). Given that the 5′ end of the guide strand is anchored, and a helical conformation is adopted by the duplex except for the first nt on the guide strand in the *Af*-Piwi-siRNA complex (Parker et al., 2005; Ma et al., 2005), a fixed distance separates the mRNA cleavage site from the anchored 5′ nt of the guide strand. The model of the *Aa*-Ago complex precisely positions the cleavable phosphate on the mRNA strand, opposite the divalent cation-mediated DD-containing catalytic motif (Figure S4B). Indeed, mutations of key residues lining the putative 5′ end binding pocket in hAgo2 have been shown to impact on mRNA cleavage activity (Ma et al., 2005). It is noteworthy that site-specific cleavage is observed at the same position for DNA guide strand-mediated cleavage by *Aa*-Ago and RNA guide strand-mediated cleavage by hAgo2 (Figure 5).

Positioning Guide DNA-mRNA Duplex between the N and PAZ Domians

The duplex segment toward the 3′ end of the guide strand (residues 15–21) and the 5′ end of the mRNA strand threads its way between the N and PAZ domains in our model of the complex (Figure S4D). This threading requires rotation/translation movements of the PAZ domain away from the N domain, on proceeding from the crystal structure of free *Aa*-Ago to its alignment in the model of the complex. The phosphates toward the 3′ end of the guide strand and the 5′ end of the paired message are anchored through interactions with basic residues on the N domain (Figure S4D), including those constituting the basic patch highlighted in Figure 3A.

Previous research has established that as many as nine contiguous noncanonical pairs can be tolerated within the duplex segment toward the 3′ end of the guide strand (Haley and Zamore, 2004). The proposed movement of the PAZ domain relative to the N domain on proceeding from the structure of *Aa*-Ago (Figure S7A) to our model of the complex (Figure S7B) suggests that helical distortions resulting from noncanonical pair formation could be tolerated by further adjustment of the relative separation between the PAZ and N domains.

Comparison of Models of *Aa*-Ago and *Pf*-Ago with Bound Duplexes

There are distinct differences between proposed models of the *Aa*-Ago (this study) and *Pf*-Ago (Song et al., 2004) complexes with guide strand-mRNA duplexes. First, our modeling studies have focused on complexes of *Aa*-Ago with a guide DNA-mRNA duplex, based on the results of filter binding and cleavage assays, in contrast to *Pf*-Ago, where complexes were proposed solely with a dsRNA duplex. Second, our stereochemically robust model of the *Aa*-Ago complex anchors the guide strand through its 5′ end within the basic pocket of the Mid domain, in contrast to anchoring the 3′ end of the guide strand in the PAZ pocket in the docking model of the *Pf*-Ago complex. This impacts on the positioning of the nucleic acid duplex that, together with the anchoring of opposite ends, is distinctly different for the proposed models of the *Aa*-Ago and *Pf*-Ago complexes. Third, biochemical experiments (Elbashir et al., 2001a, 2001b) establish that the distance ruler marking the mRNA cleavages site uses the anchored 5′ end of the guide strand as its reference, consistent with our model of the complex.

Catalytic Cycle Model of Guide Strand-Mediated mRNA Binding, Cleavage, and Release

We propose a four-step catalytic cycle model of guide strand-mediated mRNA binding, cleavage, and release within the context of the Ago scaffold in RISC. Conformer I (Figure 7) corresponds to guide strand bound Ago and involves anchoring both guide strand ends through insertion of its 5′ phosphate and adjacent base into the basic pocket of the Mid domain (Parker et al., 2005; Ma et al., 2005) and insertion of its 2 nt 3′ end into the aromatic-lined pocket of the PAZ domain (Ma et al., 2004; Lingel et al., 2004). We anticipate that the bound guide strand is unwound toward its 3′ end, with

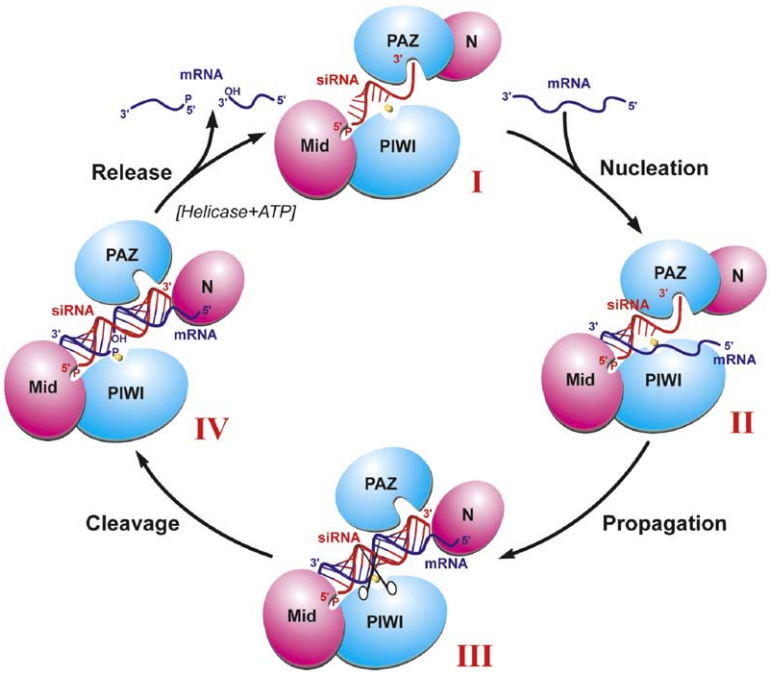

Figure 7. A Schematic of the Reaction Cycle Involving Guide RNA-Dictated mRNA Loading, Cleavage, and Product Release within the Context of the Ago Scaffold

Conformers I, II, III, and IV are as described in the text. Transition I to II corresponds to the mRNA nucleation step, transition II to III to the mRNA propagation step, transition III to IV corresponds to the cleavage step, and transition IV to I to the product release step.

its 5′ end restricted to a helical conformation due to conformational constraints imposed by the Mid and PIWI domains (Figure S7). Conformer II (Figure 7) forms after the nucleation step, where the mRNA anneals with the accessible Watson-Crick base edges of the 5′ end of the guide strand, maximizing pairing interactions spanning approximately residues 2–8 of the guide strand. Conformer III (Figure 7) forms after the propagation step, where the rest of the mRNA zippers up to form a full-length guide strand-mRNA duplex. This would require a rotational/translational transition of the PAZ domain away from the N domain, thereby releasing the 2 nt 3′ end of the guide strand from the PAZ pocket and generating a channel between the N and PAZ domains for occupancy by the zippered up segment of the duplex. Conformer IV (Figure 7) forms after the cleavage step, where the divalent cation-coordinated DD-containing RNase H catalytic motif of the PIWI domain cleaves the phosphodiester bond on the mRNA strand precisely between residues 10 and 11, as measured from the 5′ end of the guide strand. The transition between conformer IV and return to conformer I (Figure 7) corresponds to the release step, where the cleaved mRNA strands are released, perhaps facilitated by ATP-dependent RNA helicases and a switch back of PAZ to its 2 nt 3′ end binding alignment. Several of the concepts outlined in our proposed model have been independently formulated in recent reviews on RNA interference by Tomari and Zamore (2005) and Filipowicz (2005).

These models incorporate ideas that relate to preorganization of the 5′ end when bound to the RISC, even under conditions where the 5′ nt cannot pair with the target RNA (Martinez and Tuschl, 2004; Haley and Zamore, 2004), as well as ideas that emerged from microRNA target predictions (Lewis et al., 2003, 2005) and functional (Doench et al., 2003; Doench and Sharp, 2004) and kinetic (Haley and Zamore, 2004) studies, which established that 3′ bases of small RNAs do not contribute to target binding, even when they contribute to catalytic rate.

Future Prospects

Structural research to date has focused on bacterial Ago proteins, because their mammalian counterparts are difficult to express and purify in amounts suitable for crystallization trials. Our demonstration that *Aa*-Ago not only binds most tightly to DNA at the single-strand level and DNA-RNA hybrids at the double-strand level but also cleaves RNA most efficiently when paired with a DNA guide strand template opens new opportunities for understanding the origin of these DNA-mediated processes. Further advances from a structural perspective will undoubtedly require crystallographic characterization of both bacterial and, if feasible, mammalian Ago in complex with nucleic acids, preferably trapped in different states of the catalytic cycle model (Figure 7).

Experimental Procedures

Cloning, Protein Expression, and Purification

Details of cloning, together with protocols for protein expression and purification of *Aa*-Ago and its selenomethionine-labeled counterpart, are outlined in the Supplemental Experimental Procedures.

Crystallization

The purified *Aa*-Ago protein solution together with the same molar ratio of ssRNA (rU_8) was mixed 1:1 with a well solution containing 35% polyethylene glycol 550MME, 200 mM $CaCl_2$ in 100 mM sodium cacodylate, pH 6.2 in preparation for crystallization by hanging drop vapor diffusion at 20°C. Crystals grew to a maximum size of 0.15 mm × 0.1 mm × 0.1 mm over the course of 7 days.

Data Collection

A three-wavelength MAD data set was collected on *Aa*-Ago containing seven selemomethionines on beam line 14ID at the Advanced Photon Source to 2.9 Å resolution. A total of 720 frames per wavelength of 0.5° oscillations were processed by HKL2000 (Otwinowski and Minor, 1997). The crystal belongs to space group $P2_12_12_1$ with unit cell dimensions a = 63.92 Å, b = 101.12 Å, c = 115.07 Å, and $\alpha = \beta = \gamma = 90°$ with one molecule per asymmetric unit and ~42% solvent content.

Structure Determination and Refinement

The structure was determined by multiwavelength anomalous diffraction using SHARP (de la Fortelle and Bricogne, 1997). The programs SOLVE (Terwilliger, 1997) and SHELXD (Schneider and Sheldrick, 2002) were used to locate the four selenium sites, and the program SHARP was used to find two additional sites. MAD as well as SAD phases were calculated and improved by density modification assuming a solvent content of 45% using the SHARP program. The model was built by using the program O (Jones et al., 1991) and refined using X-PLOR Version 3.851 (Brunger, 1992) with Engh and Huber parameters (Engh and Huber, 1991). The R-free set contained 5% of the reflections chosen at random. An overall anisotropic B factor was refined for the structure, and individual isotropic B factor was refined for all atoms. A bulk solvent correction was also applied. The model comprises residues 4–706. Disordered regions included loop segments 262–267, 362–366, and 426–435, and these were not included in the model.

Stereochemically Robust Model of *Aa*-Ago Guide DNA-mRNA Duplex Complex

A combination of docking, superposition of relevant crystal structures, interactive modeling, molecular mechanics, and molecular dynamics were used to generate and refine a stereochemically robust model of the *Aa*-Ago protein-guide DNA-mRNA duplex complex.

We took several different approaches to align the guide DNA-mRNA duplex within the Mid-PIWI domain of *Aa*-Ago protein. Initially, we undertook a low-resolution docking computation of the components by using the GRAMM program (Vakser, 1996). Next, we explored superpositioning the RNase H fold of the *Aa*-Ago protein on the structure of RNase H fold from HIV reverse transcriptase protein bound to a DNA-RNA hybrid duplex (Sarafianos et al., 2001). Finally, we explored protein structure alignment of the *Aa*-Ago protein onto the structure of the *Af*-Piwi protein bound to an RNA duplex (Ma et al., 2005) with the program suite DEJAVU (Kleywegt and Jones, 1997). It became clear that insertion of a standard DNA-RNA hybrid duplex into *Aa*-Ago protein, although retaining 5′ end recognition and cleavage site placement, produced substantial clashes with linker (132–167) and the PAZ domain and, to a lesser extent, with the PIWI box and the N domain. We next performed interactive modeling to resolve these clashes after analysis of flexible elements of the protein structure using the programs FIRST (graph theory) (Jacobs et al., 2001) and MolMovDB (normal mode analysis) (Echols et al., 2003) as well as the subdomain structure and protein interdomain contacts using INSIGHTII.

Comparison of the 5′ end binding pockets in *Aa*-Ago with its counterpart in the *Af*-Piwi-RNA complex (Ma et al., 2005) with DEJAVU revealed that the Mid domain in *Aa*-Ago protein is closed for accommodation of the 5′ phosphate and adjacent nt. We were able to open the 5′ end binding pocket in *Aa*-Ago by rotations of the PIWI and Mid domains with respect to their small interfacial domain (composed of three short β sheets and a short α helix). Further progression of the duplex toward the 3′ end of the guide strand was modeled by taking into account the site-specific position of the scissile phosphate on the mRNA strand with respect to the divalent cation-coordinated DD-containing catalytic cleavage site, as well as surface complementarity and minimization of intermolecular clashes. This required both bending of the long β sheet of linker L1 and the shifting of the PAZ domain, so as to both relieve steric clashes and accommodate the new position of the PAZ domain, thereby positioning it to interact with the major groove of the duplex.

Several protein-nucleic acid clashes were relieved by a cleavage and paste approach involving rmsd fitting using the INSIGHTII program. Further refinement involved constrained molecular mechanics and molecular dynamics computations with the AMBER force field implemented in the DISCOVER program of the INSIGHTII suite. Secondary structure elements of the protein were preserved, and atom positions of DNA-RNA duplex were fixed during the restrained refinement. Molecular dynamics simulations were performed for 1 pico second at 300 K. Cutoff for nonbonded interactions was set at 35 Å, charge-charge interactions in the potential energy function were modified by use of a distance-dependent dielectric constant, and one to four van der Waals interactions were scaled by 0.5. Bond, angle, and out-of-plane terms were scaled in the range two to five, depending on the particular minimization requirements, with final minimization carried out with scaling factors equal to one. The pre- and postdynamics minimization runs were stopped when the root mean square of the energy gradient reached a value 1.0 kcal mol^{-1} $Å^{-1}$ and 0.1 kcal mol^{-1} $Å^{-1}$ respectively.

Double Filter Binding Assays

The affinity of the *Aa*-Ago and its mutants with various oligonucleotides (listed in Table S1) were detected and quantitated by using a double filter binding assay (Wong and Lohman, 1993). The reactions containing 5′-^{32}P-labeled nucleic acids and proteins were applied to filters containing two membranes: a protein binding Protran BA-85 nitrocellulose membrane and a nucleic acid binding Hybond-N^+ nylon membrane. After air drying, the filters were quantitated by phosphorimaging. Details of the experimental protocols and data analysis are outlined in the Supplemental Experimental Procedures.

Cleavage Activity Assay of *Aa*-Ago

Aliquots of recombinant *Aa*-Ago (0.15 μg) were incubated with a reaction mixture containing 10 mM HEPES-KOH (pH 7.4), 100 mM NaCl, 5 mM divalent cation (added as chloride salts), 8 U of RNasin, and 0.1 μM guide strand for 30 min at either 35°C or 55°C. Then, ATP and GTP were added to a final concentration of 1 mM and 0.2 mM, respectively, together with the 5′ cap-labeled substrate. The incubation was continued for 90 min. The reaction was stopped by addition of 200 μl proteinase K (0.6 mg/ml) solution followed by phenol-chloroform extraction and ethanol precipitation. The cleavage products were resolved on an 8% denaturing PAGE gel, and radioactivity was detected by phosphorimaging. The nonself-complementary guide strands used in the assay are outlined in Table S2. Additional details are outlined in the Supplemental Experimental Procedures.

Cleavage Assays Using Chimeras of hAgo1 and hAgo2

The FLAG/HA-tagged wild-type and hAgo1/hAgo2 chimeric constructs were transiently transfected into 293 HEK cells, and hAgo2 proteins were immunoprecipitated from the cell lysates by using anti-FLAG antibody. The expression levels of the wild-type and mutant hAgo2 proteins were assessed by Western blotting using anti-HA antibody. The stringently washed beads carrying equal amounts of bound FLAG/HA-tagged hAgo2 proteins were preincubated with a single-stranded siRNA to reconstitute RISC activity. After an additional washing step to remove the unbound siRNA, the beads were incubated with a ^{32}P cap-labeled target RNA. After 1 hr and 30 min incubation, the RNA was recovered from the beads and analyzed by denaturing gel electrophoresis.

Reconstitution of RISC Activity Using Single-Stranded siRNA

The in vitro-transcribed cleavage substrate was ^{32}P cap labeled (Martinez et al., 2002), and cleavage was assayed as described previously (Meister et al., 2004) with the following modifications. 10 μl of beads were preincubated with 100 nM single-stranded, 5′-phosphorylated siRNA for 30 min at 30°C. The beads were subsequently used in a 25 μl cleavage reaction containing 1 mM ATP, 0.2 mM GTP, 10 U/ml RNasin (Promega) in 100 mM KCl, 1.5 mM $MgCl_2$, 0.5 mM DTT, and 10 mM HEPES-KOH (pH 7.9) at 30°C for 1 hr and 30 min. The reaction was stopped by addition of 200 μl proteinase K buffer followed by proteinase K treatment and RNA isolation

(Tuschl et al., 1999). The RNA was separated by 8% PAGE, and radioactivity was detected by phosphorimaging.

Supplemental Data

Supplemental Data include Supplemental Results, Supplemental Experimental Procedures, Supplemental References, seven figures, and two tables and are available with this article online at http://www.molecule.org/cgi/content/full/19/3/405/DC1/.

Acknowledgments

D.J.P. is supported by funds from the Abby Rockefeller Mauze Trust and the Dewitt Wallace and Maloris Foundations, T.T. is supported by National Institutes of Health grant R01 GM068476-01, and G.M. is an Emmy Noether fellow of the Deutsche Forschungsgemeinschaft (DFG). We would like to thank the staff at beamline 14ID of the Advanced Photon Source (APS) supported by the U.S. Department of Energy for assistance with data collection. The crystal structure of *Aa*-Ago was first presented at the Banbury Symposium on "RNAi-Related Processes in Plants: Chromatin, Development and Defense" held at Cold Spring Harbor Laboratories on August 15–18, 2004.

Received: February 21, 2005
Revised: April 6, 2005
Accepted: July 18, 2005
Published: August 4, 2005

References

Brunger, A.T. (1992). X-PLOR: A System for Crystallography and NMR, Version 3.1 (New Haven, CT: Yale University Press).

Campos-Olivas, R., Louis, J.M., Clerot, D., Gronenborn, B., and Gronenborn, A.M. (2002). The structure of replication initiator unites diverse aspects of nucleic acid metabolism. Proc. Natl. Acad. Sci. USA. *99*, 10310–10315.

Carmell, M.A., Xuan, Z., Zhang, M.Q., and Hannon, G.J. (2002). The Argonaute family: tentacles that reach into RNAi, developmental control, stem cell maintenance, and tumorigenesis. Genes Dev. *16*, 2733–2742.

Cerutti, L., Mian, N., and Bateman, A. (2000). Domains in gene silencing and cell differentiation proteins: the novel PAZ domain and redefinition of the Piwi domain. Trends Biochem. Sci. *25*, 481–482.

Chiu, Y.L., and Rana, T.M. (2003). siRNA function in RNAi: a chemical modification analysis. RNA *9*, 1034–1048.

Davies, D.R., Goryshin, I.Y., Reznikoff, W.S., and Rayment, I. (2000). Three-dimensional structure of the Tn5 synaptic complex transposition intermediate. Science *289*, 77–85.

de la Fortelle, E., and Bricogne, G. (1997). Maximum-likelihood heavy-atom parameter refinement for multiple isomorphous and multiwavelength anomalous diffraction methods. Methods Enzymol. *276*, 472–494.

Doench, J.G., and Sharp, P.A. (2004). Specificity of microRNA target selection in translation repression. Genes Dev. *18*, 504–511.

Doench, J.G., Petersen, C.P., and Sharp, P.A. (2003). siRNAs can function as miRNAs. Genes Dev. *17*, 438–442.

Echols, N., Milburn, D., and Gerstein, M. (2003). MolMovDB: analysis and visualization of conformational change and structural flexibility. Nucleic Acids Res. *31*, 478–482.

Elbashir, S.M., Lendeckel, W., and Tuschl, T. (2001a). RNA interference is mediated by 21- and 22-nucleotide RNAs. Genes Dev. *15*, 188–200.

Elbashir, S.M., Martinez, J., Patkaniowska, A., Lendeckel, W., and Tuschl, T. (2001b). Functional anatomy of siRNAs for mediating efficient RNAi in *Drosophila melanogaster* embryo lysate. EMBO J. *20*, 6877–6888.

Engh, R.A., and Huber, R. (1991). Accurate bond and angle parameters for X-ray protein structure refinement. Acta Crystallogr. A *47*, 381–392.

Evans, S.P., and Bycroft, M. (1999). NMR structure of the N-terminal domain of *S. cerevisiae* RNase H1 reveals a fold with a strong resemblance to the N-terminal domain of ribosomal protein L9. J. Mol. Biol. *291*, 661–669.

Filipowicz, W. (2005). RNAi: the nuts and bolts of the RISC machine. Cell *122*, 17–20.

Friedman, A.M., Fishmann, T.O., and Steitz, T.A. (1995). Crystal structure of lac repressor core tetramer and its implications for DNA looping. Science *268*, 1721–1727.

Haley, B., and Zamore, P.D. (2004). Kinetic analysis of RNAi enzyme complex. Nat. Struct. Mol. Biol. *11*, 599–606.

Hammond, S.M., Boettcher, S., Caudy, A.A., Kobayashi, R., and Hannon, G.J. (2001). Argonaute2, a link between genetic and biochemical analyses of RNAi. Science *293*, 1146–1150.

Hutvagner, G., and Zamore, P.D. (2002). A microRNA in a multiple turnover RNAi enzyme complex. Science *297*, 2056–2060.

Jacobs, D.J., Rader, A.J., Kuhn, L.A., and Thorpe, M.F. (2001). Protein flexibility predictions using graph theory. Proteins *44*, 150–165.

Jones, T.A., Zou, J.Y., and Cowan, S.W. (1991). Improved methods for building protein models in electron density maps and the location of errors in these models. Acta Crystallogr. A *47 (Pt 2)*, 110–119.

Kleywegt, G.J., and Jones, T.A. (1997). Detecting folding motifs and similarities in protein structures. Methods Enzymol. *277*, 525–545.

Lai, L., Yokota, H., Hung, L.W., Kim, R., and Kim, S.H. (2000). Crystal structure of archael RNase Hii: A homologue of human major Rnase H. Structure *8*, 897–904.

Lewis, B.P., Shih, I.-h., Jones-Rhoades, M.W., Bartel, D.P., and Burge, C.B. (2003). Prediction of mammalian miroRNA targets. Cell *115*, 787–798.

Lewis, B.P., Burge, C.B., and Bartel, D.P. (2005). Conserved seed pairing, often flanked by adenosines, indicates that thousands of human genes are micrRNA targets. Cell *120*, 15–20.

Lima, W.F., Wu, H., Nichols, J.G., Prakash, T.P., Ravikumar, V., and Crooke, S.T. (2003). Human RNase H1 uses one trytophan and two lysines to position the enzyme at the 3′-DNA/5′-RNA terminus of the heteroduplex substrate. J. Biol. Chem. *278*, 49860–49867.

Lingel, A., Simon, B., Izaurralde, E., and Sattler, M. (2003). Structure and nucleic-acid binding of the Drosophila Argonaute 2 PAZ domain. Nature *426*, 465–469.

Lingel, A., Simon, B., Izaurralde, E., and Sattler, M. (2004). Nucleic acid 3′-end recognition by the Argonaute2 PAZ domain. Nat. Struct. Mol. Biol. *11*, 576–577.

Liu, J., Carmell, M.A., Rivas, F.V., Marsden, C.G., Thompson, J.M., Song, J.J., Hammond, S.M., Joshua-Tor, L., and Hannon, G.J. (2004). Argonaute2 is the catalytic engine of mammalian RNAi. Science *305*, 1437–1441.

Ma, J.B., Ye, K., and Patel, D.J. (2004). Structural basis for overhang-specific small interfering RNA recognition by the PAZ domain. Nature *429*, 318–322.

Ma, J.B., Yuan, Y.R., Meister, G., Pei, Y., Tuschl, T., and Patel, D.J. (2005). Structural basis for 5′-end-specific recognition of the guide RNA strand by *A. fulgidus* PIWI protein. Nature *434*, 666–670.

Mallory, A.C., Reinhart, B.J., Jones-Rhoades, M.W., Tang, G., Zamore, P.D., Barton, M.K., and Bartel, D.P. (2004). MicroRNA control of PHABULOSA in leaf development: importance of pairing to the microRNA 5′-region. EMBO J. *23*, 3356–3364.

Martinez, J., and Tuschl, T. (2004). RISC is a 5′ phosphomonoester-producing RNA endonuclease. Genes Dev. *18*, 975–980.

Martinez, J., Patkaniowska, A., Urlaub, H., Luhrmann, R., and Tuschl, T. (2002). Single-stranded antisense siRNAs guide target RNA cleavage in RNAi. Cell *110*, 563–574.

Meister, G., and Tuschl, T. (2004). Mechanisms of gene silencing by double-stranded RNA. Nature *431*, 343–349.

Meister, G., Landthaler, M., Patkaniowska, A., Dorsett, Y., Teng, G., and Tuschl, T. (2004). Human argonaute2 mediates RNA cleavage targeted by miRNAs and siRNAs. Mol. Cell *15*, 185–197.

Otwinowski, Z., and Minor, W. (1997). Processing of x-ray diffrac-

tion data collected in oscillation mode. Methods Enzymol. *276*, 307–326.

Parker, J.S., Roe, S.M., and Barford, D. (2004). Crystal structure of a PIWI protein suggests mechanisms for siRNA recognition and slicer activity. EMBO J. *23*, 4727–4737.

Parker, J.S., Roe, S.M., and Barford, D. (2005). Structural insights into mRNA recognition from a PIWI-domain-siRNA-guide complex. Nature *434*, 663–666.

Rivas, F.V., Tolia, N.H., Song, J.J., Aragon, J.P., Liu, J., Hannon, G.J., and Joshua-Tor, L. (2005). Purified Argonaute2 and an siRNA form recombinant human RISC. Nat. Struct. Mol. Biol. *12*, 340–349.

Sarafianos, S.G., Das, K., Tantillo, C., Clark, A.D., Jr., Ding, J., Whitcomb, J.M., Boyer, P.L., Hughes, S.H., and Arnold, E. (2001). Crystal structure of HIV-1 reverse transcriptase in complex with a polypurine tract RNA:DNA. EMBO J. *20*, 1449–1461.

Schneider, T.R., and Sheldrick, G.M. (2002). Substructure solution with SHELEXD. Acta Crystallogr. D. *58*, 1772–1779.

Schwarz, S.S., Tomari, Y., and Zamore, P.D. (2004). The RNA-induced silencing complex is a Mg^{2+}-dependent endonuclease. Curr. Biol. *14*, 787–791.

Song, J.J., Liu, J., Tolia, N.H., Schneiderman, J., Smith, S.K., Martienssen, R.A., Hannon, G.J., and Joshua-Tor, L. (2003). The crystal structure of the Argonaute2 PAZ domain reveals an RNA binding motif in RNAi effector complexes. Nat. Struct. Biol. *10*, 1026–1032.

Song, J.J., Smith, S.K., Hannon, G.J., and Joshua-Tor, L. (2004). Crystal structure of Argonaute and its implications for RISC slicer activity. Science *305*, 1434–1437.

Sontheimer, E.J. (2005). Assembly and function of RNA silencing complexes. Nat. Rev. Mol. Cell Biol. *6*, 127–138.

Stark, A., Brennecke, J., Russel, R.B., and Cohen, S.M. (2003). Identification of Drosophila microRNA targets. PLoS Biol. *1*, 397–409.

Tahbaz, N., Kolb, F.A., Zhang, H., Jaronczyk, K., Filipowicz, W., and Hobman, T.C. (2004). Characterization of the interactions between mammalian PAZ PIWI domain proteins and Dicer. EMBO Rep. *5*, 1–6.

Terwilliger, T.C. (1997). Multiwavelength anomalous diffraction phasing of macromolecular structures: analysis of MAD data as single isomorphous replacement with anomalous scattering data using the MADMRG Program. Methods Enzymol. *276*, 530–537.

Tomari, Y., and Zamore, P.D. (2005). Perspective: machine for RNAi. Genes Dev. *19*, 517–529.

Tuschl, T., Zamore, P.D., Lehmann, R., Bartel, D.P., and Sharp, P.A. (1999). Targeted mRNA degradation by double-stranded RNA in vitro. Genes Dev. *13*, 3191–3197.

Vakser, I.A. (1996). Low resolution docking: prediction of complexes for underdetermined structures. Biopolymers *39*, 455–464.

Wong, I., and Lohman, T.M. (1993). A double-filter method for nitrocellulose-filter binding: Application to protein-nucleic acid interactions. Proc. Natl. Acad. Sci. USA *90*, 5428–5432.

Yan, K.S., Yan, S., Farooq, A., Han, A., Zeng, L., and Zhou, M.M. (2003). Structure and conserved RNA binding of the PAZ domain. Nature *426*, 468–474.

Yang, W., and Steitz, T.A. (1995). Recombining the structures of HIV integrase, RuvC and RNase H. Structure *3*, 131–134.

Accession Numbers

Coordinates have been deposited in the Protein Data Bank under the following accession codes: X-ray structure of *Aa*-Ago, 1YVU, and model of *Aa*-Ago complexed with guide DNA and mRNA, 2ADS.